strain
An International Journal for Experimental Mechanics

Compositional and Microchemical Evidence of Piezonuclear Fission Reactions in Rock Specimens Subjected to Compression Tests

A. Carpinteri*, A. Chiodoni†, A. Manuello* and R. Sandrone‡

*Politecnico di Torino, Department of Structural Engineering & Geotechnics, Corso Duca degli Abruzzi 24, 10129 Torino, Italy

†Italian Institute of Technology, Center for Space Human Robotics, Corso Trento 21, 10129 Torino, Italy

‡Politecnico di Torino, Department of Land, Environment and Geo-Engineering, Corso Duca degli Abruzzi 24, 10129 Torino, Italy

ABSTRACT: Energy-dispersive X-ray spectroscopy (EDS) is performed on different samples of external or fracture surfaces belonging to specimens used in piezonuclear tests [*Strain* 45, 2009, 332; *Strain* (in press); Phys. Lett. A. 373, 2009, 4158]. For each sample, different measurements of the same crystalline phases (phengite or biotite) are performed to obtain averaged information of the chemical composition and to detect possible piezonuclear transmutations from iron to lighter elements. The samples were carefully chosen to investigate and compare the same minerals both before and after the crushing failure. Phengite and biotite, which are quite common in the Luserna stone (20 and 2%, respectively), are considered owing to the high iron concentration in their chemical compositions. The results of EDS analyses show that, on the fracture surface samples, a considerable reduction in the iron content (~25%) is counterbalanced by an increase in Al, Si, and Mg concentrations.

KEY WORDS: *compressive tests, energy-dispersive X-ray spectroscopy, piezonuclear reactions*

Introduction

It has been shown that pressure, exerted on radioactive or inert media, can generate nuclear reactions and reproducible neutron emissions. In particular, low-energy nuclear reactions and heat generation have been verified in pressurised deuterium gas by Arata *et al.* [1, 2] and in radioactive deuterium-containing liquids during ultrasounds and cavitation by Taleyarkhan *et al.* [3]. The experiments recently proposed by Carpinteri *et al.* [4] and by Cardone *et al.* [5] follow a different path from those of other research teams and represent the first evidence of piezonuclear reactions and neutron emissions in inert, stable and non-radioactive solids under compression, as well as in non-radioactive liquids during ultrasound cavitation [6, 7]. The analyses of this paper are in strict connection with the results of piezonuclear tests presented by Carpinteri *et al.* [4, 8] and by Cardone *et al.* [5].

Neutron emission measurements, by means of helium-3 neutron detectors, have recently been performed on solid test specimens during crushing failure [4, 5]. Neutron emissions from 'Luserna stone' test specimens were found to be of about one order of magnitude higher than the natural background level at the time of failure. These neutron emissions should be caused by nucleolysis or piezonuclear 'fissions' occurred in the granitic gneiss samples, transforming heavier (Fe) into lighter (Mg, Al, Si) atoms in correspondence to brittle failure of the specimens. These reactions – less infrequent than we could think – would be activated where the environment conditions (pressure and temperature) are particularly severe, and mechanical phenomena of fracture, crushing, fragmentation, comminution, erosion, friction, etc., may occur [4, 5, 8].

In this paper, energy-dispersive X-ray spectroscopy (EDS) is described on different samples of external or fracture surfaces belonging to the same two specimens used in the piezonuclear tests by Carpinteri *et al.* [4, 5] to correlate the neutron emission from the Luserna stone with the variations in rock composition due to brittle failure of the granitic gneiss specimens. These analyses lead to obtain averaged information of the mineral chemical composition and to detect possible piezonuclear transmutations from iron to lighter elements. The quantitative elemental analyses were performed by a ZEISS Supra 40 field emission scanning electron microscope (FESEM) equipped with an Oxford X-ray microanalysis. The samples were carefully chosen to investigate and

doi: 10.1111/j.1475-1305.2010.00767.x

compare the same crystalline phases both before and after the crushing failure. In particular, two crystalline phases, phengite and biotite, were considered because of their high iron content and relative abundances in the Luserna stone (20 and 2%, respectively) (see Figure 1A,B) [9].

Granitic Gneiss Composition and Piezonuclear Test

Luserna stone is a leucogranitic orthogneiss, probably from the Lower Permian Age, that outcrops in the Luserna-Infernotto basin (Cottian Alps, Piedmont) at the border between the Turin and Cuneo provinces (north-western Italy) [10]. Characterised by a micro 'Augen' texture, it is grey-greenish or locally pale blue in colour. Geologically, Luserna stone pertains to the Dora-Maira Massif [9, 11] that represents a part of the ancient European margin annexed to the Cottian Alps during Alpine orogenesis. From a petrographic point of view, it is the metamorphic result of a late-Ercinian leucogranitic rock transformation [9, 12] The Luserna Stone has a sub-horizontal attitude, with a marked fine-grained foliation that is mostly associated with visible lineation. The mineralogical composition includes K-feldspar (10–25 wt. %), quartz (30–40 wt. %), albite (15–25 wt. %) and phengite (10–20 wt. %); subordinated biotite, chlorite, zoisite and/or clinozoisite/epidote (<5%). In addition to common accessory phases (ores, titanite, apatite and zircon), tourmaline, carbonates, rare axinite and frequent fluorite are present [9, 13].

In the fundamental papers of Carpinteri *et al.* [4] and Cardone *et al.* [5], the materials selected for the compression tests were Carrara marble and Luserna stone. This choice was prompted by the consideration that, test specimen dimensions being the same, different brittleness numbers [14] would cause catastrophic failure in granite, not in marble. These early results on piezonuclear reactions from brittle fracture of Luserna stone specimens may be accounted for by the catastrophic nature of the failure [14–16]. In this case, another important aspect that should be taken into account is also the composition of the materials in which the piezonuclear reactions have occurred. The marble used in the piezonuclear tests [4, 5] contains only iron impurities (not more than 0.07% of Fe_2O_3 as total Fe), where as Luserna stone contains a considerable amount of iron oxides (~3% of Fe_2O_3 as total Fe). The iron content of the Luserna granite used in the piezonuclear experiments could contribute to the phenomenon in question, in analogy with the case of piezonuclear reactions in liquids [6, 7]. Piezonuclear reactions with neutron emissions have in fact been obtained in liquids containing iron chloride or iron nitrate and subjected to ultrasounds and cavitation [6, 7]. In these experiments on liquid solutions, aluminium atoms appeared at the end in a final quantity as large as about seven times the small initial quantity. For this reason, the iron content in the Luserna stone must be considered, together with the brittle nature of failures, as a very important factor for the occurrence of piezonuclear reactions and neutron flux emissions. In this context, the

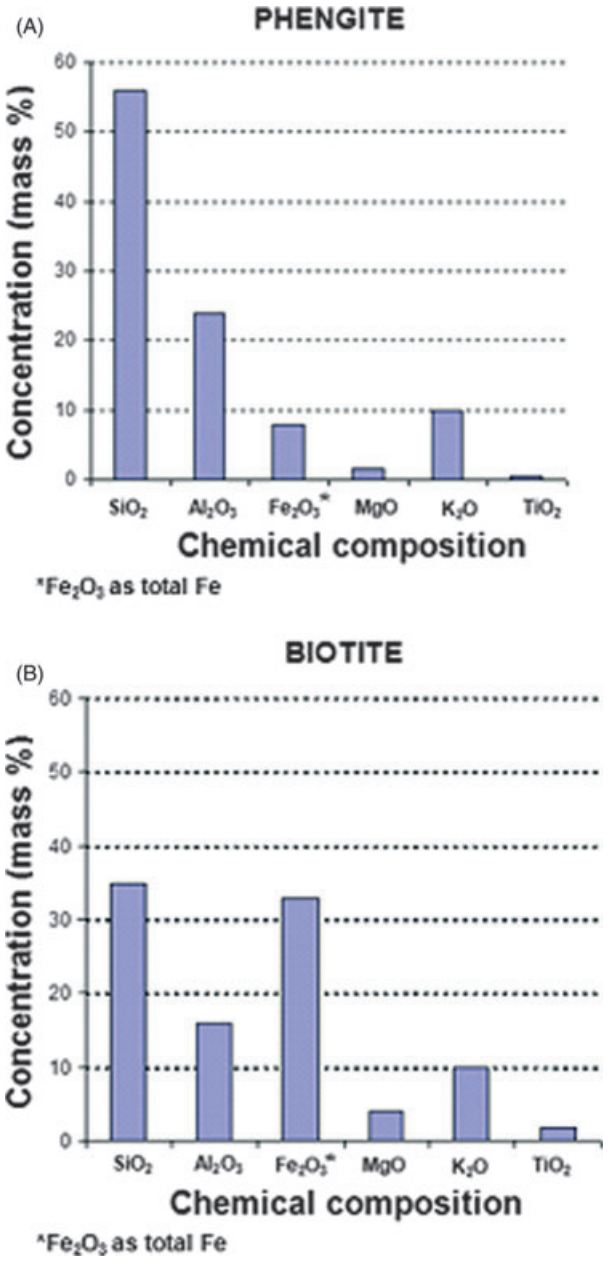

Figure 1: (A) The chemical composition of phengite includes the following: SiO_2 (~56%), Al_2O_3 (~24%), Fe_2O_3 and FeO (~8%), MgO (~1.5%), Na_2O (~0.2%) and K_2O (~10%). (B) The chemical composition of biotite includes the following: SiO_2 (~35%), Al_2O_3 (~16%), Fe_2O_3 and FeO (~33%), MgO (~3.5%), TiO_2 (~1.5%) and K_2O (~10%)

doi: 10.1111/j.1475-1305.2010.00767.x

compositional variations found between external and fracture surfaces may be particularly important to assess 'nucleolysis' or piezonuclear 'fissions', occurred in the tested material, transforming heavier (Fe) into lighter (Mg, Al, Si) atoms.

X-ray Spectroscopy Analysis

To correlate the composition of Luserna stone with the neutron emission from the fracture surfaces, semi-quantitative compositional analyses were carried out by means of a ZEISS Supra 40 FESEM equipped with an Oxford INCA energy-dispersive X-ray detector (Si(Li)) with a resolution of 133 eV @ (MnKα). Each sample was carefully chosen and preliminarily characterised by using an optical microscope to precisely find the minerals of interest, i.e. biotite and phengite. The samples were covered by a 5-nm-thick Cr layer to improve their conductivity and properly distinguish the phases of interest. The energy used for the analyses was 20 KeV.

Using a nanometric electron beam probe, the measurements were carried out on different zones of the samples. This kind of analysis involves tenths of cubic microns for each acquisition point in the investigated sample.

Two different kinds of samples were examined: (i) polished thin sections, finished with a standard petrographic sample procedure, covered by Cr, for what concerns the external surface of the Luserna stone; (ii) small portions of fracture surfaces without any kind of preparation, apart from the Cr covering to avoid any kind of modification of the composition due to the slice preparation, for what concerns the fracture surface.

Semi-quantitative standardless analysis was performed on the collected spectra, fixing the stoichiometry of the oxides, to correlate the oxides content with the specific crystalline phase. The Cr lines were excluded from the semi-quantitative evaluation.

In Figure 2A, two polished thin sections obtained from the external surfaces of an integer and uncracked portion of the specimen are shown. The polished thin sections present a rectangular geometry (45 × 27 mm) and are 30 μm thick. In Figure 2B,

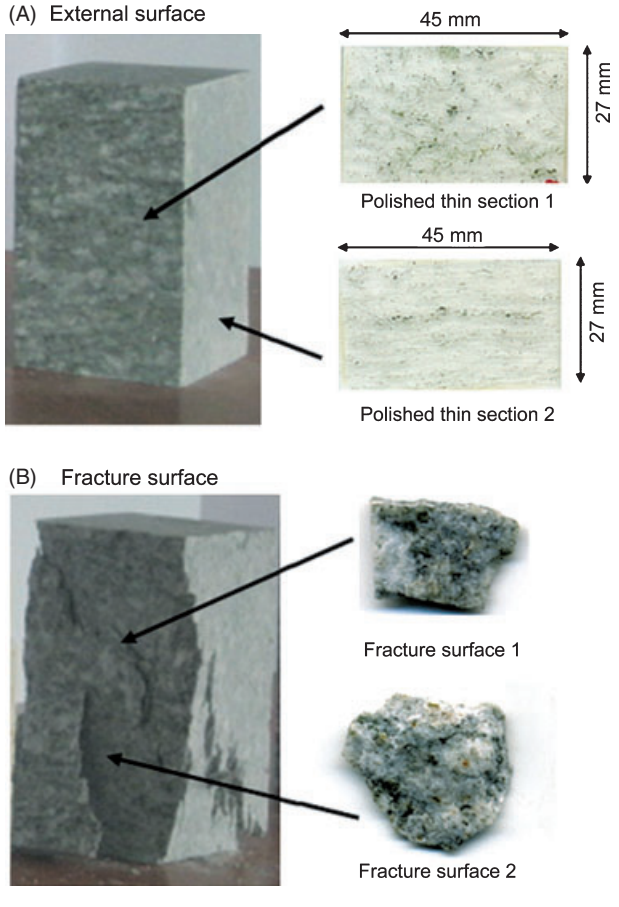

Figure 2: (A) Polished thin sections obtained by the external surface of an integer and not fractured portion of the tested specimens [4, 5]. (B) Fracture surface belonging to the tested specimens [4, 5]

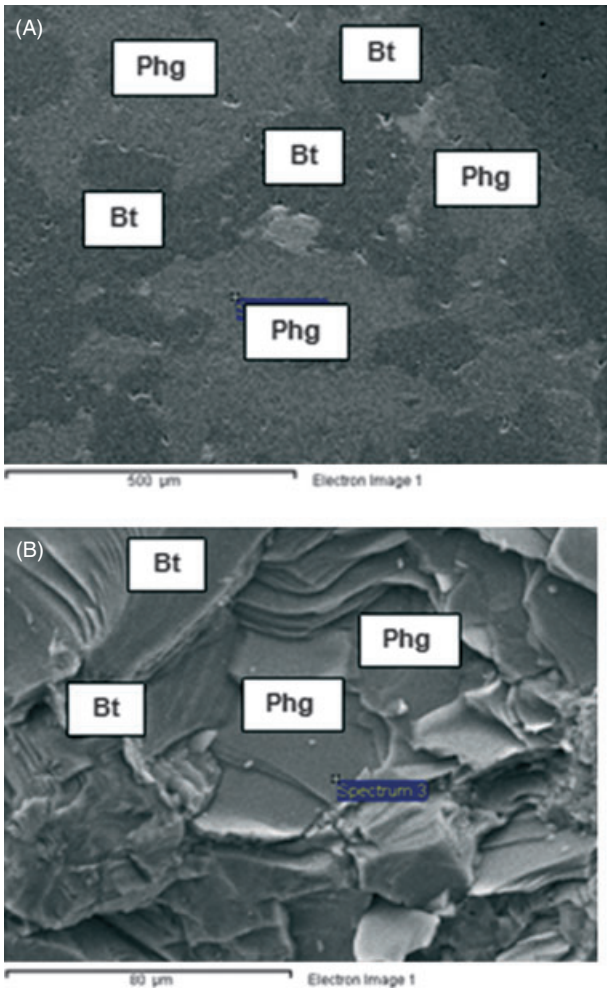

Figure 3: Field emission scanning electron microscope images of phengite and biotite in the case of (A) external and (B) fracture sample

doi: 10.1111/j.1475-1305.2010.00767.x

Table 1: Chemical analyses (wt. %) and atomic proportions (basis 22 oxygens) for phengite on external surfaces

	1	2	3	4	5	6	7	8	9	10
SiO_2	56.94	57.06	56.12	54.52	56.60	56.62	56.83	56.80	55.83	54.58
TiO_2	0.00	0.00	0.00	0.17	0.00	0.16	0.00	0.00	0.00	0.30
Al_2O_3	25.50	26.30	22.57	23.34	23.20	23.73	23.45	23.44	25.45	24.80
FeO	7.63	8.69	9.40	7.70	8.23	8.69	8.80	8.90	8.91	8.08
MgO	1.49	1.34	1.87	1.52	1.63	1.34	1.40	1.40	1.40	0.92
CaO	0.00	0.00	0.00	0.00	0.00	0.00	0.00	0.00	0.00	0.00
Na_2O	0.00	0.24	0.00	0.00	0.10	0.00	0.00	0.06	0.00	0.62
K_2O	10.39	10.53	10.71	10.33	10.25	10.24	10.22	10.21	10.22	11.15
Si	7.32	7.35	7.28	7.01	7.32	7.28	7.31	7.30	7.11	6.98
Al^{IV}	0.68	0.65	0.72	0.99	0.68	0.73	0.69	0.70	0.89	0.75
Al^{VI}	2.84	2.82	2.73	3.00	2.85	2.87	2.86	2.85	2.93	2.80
Ti	0.00	0.00	0.00	0.02	0.00	0.02	0.00	0.00	0.00	0.03
Fe	0.82	0.94	1.02	0.83	0.89	0.93	0.95	0.96	0.95	0.90
Mg	0.29	0.26	0.36	0.29	0.31	0.26	0.27	0.27	0.27	0.18
Ca	0.00	0.00	0.00	0.00	0.00	0.00	0.00	0.00	0.00	0.00
Na	0.00	0.06	0.00	0.00	0.03	0.00	0.00	0.02	0.00	0.16
K	1.71	1.73	1.77	1.69	1.69	1.68	1.68	1.67	1.66	1.89
	11	12	13	14	15	16	17	18	19	20
SiO_2	56.94	57.06	56.12	54.52	56.60	56.62	56.83	56.80	57.02	55.02
TiO_2	0.00	0.00	0.00	0.00	0.50	0.16	0.00	0.00	0.16	0.50
Al_2O_3	24.90	24.01	22.57	26.34	23.20	23.73	23.45	23.44	23.04	24.51
FeO	7.60	7.94	8.63	7.03	8.23	7.92	8.10	8.09	7.87	8.23
MgO	1.49	1.34	1.13	1.52	1.63	1.34	1.40	1.40	1.31	1.86
CaO	0.00	0.00	0.00	0.00	0.00	0.00	0.00	0.00	0.00	0.00
Na_2O	0.00	0.24	0.00	0.09	0.10	0.24	0.00	0.06	0.00	0.22
K_2O	10.39	10.53	10.71	10.33	10.25	10.24	10.22	10.21	10.76	9.71
Si	7.35	7.38	7.36	7.04	7.21	7.29	7.33	7.33	7.36	7.20
Al^{IV}	0.65	0.62	0.65	0.96	0.79	0.71	0.67	0.67	0.64	0.80
Al^{VI}	2.88	2.86	2.84	3.05	2.85	2.89	2.90	2.90	2.87	2.85
Ti	0.00	0.00	0.00	0.00	0.05	0.02	0.00	0.00	0.02	0.05
Fe	0.81	0.86	0.95	0.76	0.88	0.85	0.87	0.87	0.85	0.87
Mg	0.29	0.26	0.22	0.29	0.31	0.26	0.27	0.27	0.25	0.35
Ca	0.00	0.00	0.00	0.00	0.00	0.00	0.00	0.00	0.00	0.00
Na	0.00	0.06	0.00	0.02	0.03	0.06	0.00	0.02	0.00	0.05
K	1.71	1.74	1.79	1.70	1.67	1.68	1.68	1.68	1.77	1.57
	21	22	23	24	25	26	27	28	29	30
SiO_2	56.94	57.06	56.12	56.60	56.62	56.83	56.80	56.94	57.06	56.12
TiO_2	0.00	0.00	0.00	0.00	0.16	0.00	0.00	0.00	0.00	0.00
Al_2O_3	23.17	22.89	22.57	23.20	23.73	23.45	24.90	23.17	22.89	22.57
FeO	8.81	8.69	9.40	8.23	8.69	8.80	8.90	8.81	8.69	9.40
MgO	1.49	1.34	1.87	1.63	1.34	1.40	1.40	1.49	1.34	1.87
CaO	0.00	0.00	0.00	0.00	0.00	0.00	0.00	0.00	0.00	0.00
Na_2O	0.00	0.24	0.00	0.10	0.00	0.00	0.06	0.00	0.24	0.00
K_2O	10.39	10.53	10.71	10.25	10.24	10.22	10.21	10.39	10.53	10.71
Si	7.32	7.35	7.28	7.32	7.28	7.31	7.30	7.32	7.35	7.28
Al^{IV}	0.68	0.65	0.72	0.68	0.73	0.69	0.70	0.68	0.65	0.72
Al^{VI}	2.84	2.82	2.73	2.85	2.87	2.86	2.85	2.84	2.82	2.73
Ti	0.00	0.00	0.00	0.00	0.02	0.00	0.00	0.00	0.00	0.00
Fe	0.95	0.94	1.02	0.89	0.93	0.95	0.96	0.95	0.94	1.02
Mg	0.29	0.26	0.36	0.31	0.26	0.27	0.27	0.29	0.26	0.36
Ca	0.00	0.00	0.00	0.00	0.00	0.00	0.00	0.00	0.00	0.00
Na	0.00	0.06	0.00	0.03	0.00	0.00	0.02	0.00	0.06	0.00
K	1.71	1.73	1.77	1.69	1.68	1.68	1.67	1.71	1.73	1.77

doi: 10.1111/j.1475-1305.2010.00767.x

Table 2: Chemical analyses (wt. %) and atomic proportions (basis 22 oxygens) for phengite on fracture surfaces

	1	2	3	4	5	6	7	8	9	10
SiO_2	54.02	54.43	52.60	53.65	52.84	55.62	56.81	55.66	55.14	59.57
TiO_2	0.00	0.00	0.00	0.16	0.20	0.00	0.16	0.00	0.00	0.50
Al_2O_3	27.51	26.38	27.33	27.16	30.17	26.23	28.26	27.79	27.04	25.52
FeO	6.67	6.91	7.39	7.16	5.67	6.47	3.05	4.87	5.98	4.88
MgO	1.86	1.40	1.38	1.61	1.04	1.52	1.13	0.95	1.91	1.19
CaO	0.00	0.00	0.00	0.00	0.00	0.00	0.00	0.00	0.00	0.00
Na_2O	0.22	0.00	0.19	0.24	0.17	0.89	0.20	0.27	0.00	0.57
K_2O	9.71	9.88	10.11	10.01	9.91	9.26	10.55	10.47	9.94	9.37
Si	6.93	7.06	6.87	6.92	6.76	7.11	7.14	7.08	7.04	7.39
Al^{IV}	1.07	0.94	1.13	1.08	1.25	0.89	0.86	0.92	0.96	0.61
Al^{VI}	3.09	3.09	3.08	3.05	3.30	3.07	3.33	3.25	3.11	3.12
Fe	0.72	0.75	0.81	0.77	0.61	0.69	0.32	0.52	0.64	0.51
Mg	0.36	0.27	0.27	0.31	0.20	0.29	0.21	0.18	0.36	0.22
Ca	0.00	0.00	0.00	0.00	0.00	0.00	0.00	0.00	0.00	0.00
Na	0.06	0.00	0.05	0.06	0.04	0.22	0.05	0.07	0.00	0.14
K	1.59	1.63	1.69	1.65	1.62	1.51	1.69	1.70	1.62	1.48
	11	12	13	14	15	16	17	18	19	20
SiO_2	57.00	56.56	55.88	56.53	55.53	57.53	55.78	56.43	54.84	56.62
TiO_2	0.00	0.00	0.00	0.00	0.00	0.00	0.18	0.00	0.00	0.00
Al_2O_3	27.52	24.70	25.31	24.53	26.53	26.53	26.95	25.38	29.87	25.23
FeO	4.35	6.56	6.11	6.85	4.40	6.40	5.12	6.91	4.67	6.47
MgO	1.13	1.47	1.79	1.33	1.20	1.20	1.30	1.40	1.04	1.52
CaO	0.00	0.00	0.00	0.00	0.00	0.00	0.00	0.00	0.00	0.00
Na_2O	0.57	0.00	0.00	0.00	0.00	0.00	0.15	0.00	0.17	0.89
K_2O	9.41	10.71	10.91	10.76	12.51	12.51	10.52	9.88	9.91	8.26
Si	7.41	7.26	7.18	7.27	7.15	7.15	7.11	7.22	6.88	7.26
Al^{IV}	0.59	0.74	0.82	0.73	0.85	0.85	0.89	0.78	1.12	0.74
Al^{VI}	3.23	3.00	3.01	2.99	3.03	3.03	3.16	3.05	3.30	3.07
Fe	0.45	0.71	0.66	0.74	0.67	0.67	0.55	0.74	0.60	0.69
Mg	0.21	0.28	0.34	0.26	0.22	0.22	0.25	0.27	0.20	0.29
Ca	0.00	0.00	0.00	0.00	0.00	0.00	0.00	0.00	0.00	0.00
Na	0.14	0.00	0.00	0.00	0.00	0.00	0.04	0.00	0.04	0.22
K	1.47	1.76	1.79	1.77	1.98	1.98	1.71	1.61	1.59	1.35
	21	22	23	24	25	26	27	28	29	30
SiO_2	54.52	54.02	55.43	54.52	56.60	56.62	56.83	56.80	55.02	56.43
TiO_2	0.17	0.00	0.00	0.17	0.00	0.16	0.00	0.00	0.00	0.00
Al_2O_3	28.34	27.51	27.38	28.34	27.20	27.73	28.45	29.44	28.51	28.38
FeO	5.70	6.67	5.91	5.20	3.23	4.69	4.80	5.90	5.67	4.91
MgO	1.52	1.86	1.40	1.52	1.63	1.34	1.40	1.40	1.86	1.40
CaO	0.00	0.00	0.00	0.00	0.00	0.00	0.00	0.00	0.00	0.00
Na_2O	0.00	0.22	0.00	0.00	0.10	0.00	0.00	0.06	0.22	0.00
K_2O	10.33	9.71	9.88	10.33	11.25	10.24	10.22	10.21	9.71	9.88
Si	6.93	6.93	7.07	6.93	7.17	7.12	7.08	6.97	7.03	7.07
Al^{IV}	1.07	1.07	0.94	1.07	0.83	0.88	0.92	1.03	0.97	0.93
Al^{VI}	3.18	3.09	3.18	3.18	3.23	3.23	3.26	3.23	3.18	3.27
Fe	0.61	0.72	0.63	0.61	0.34	0.49	0.50	0.61	0.59	0.52
Mg	0.29	0.36	0.27	0.29	0.31	0.25	0.26	0.26	0.34	0.26
Ca	0.00	0.00	0.00	0.00	0.00	0.00	0.00	0.00	0.00	0.00
Na	0.00	0.06	0.00	0.00	0.03	0.00	0.00	0.01	0.05	0.00
K	1.68	1.59	1.61	1.68	1.82	1.64	1.62	1.60	1.53	1.58

doi: 10.1111/j.1475-1305.2010.00767.x

Table 3: Chemical analyses (wt. %) and atomic proportions (basis 22 oxygens) for biotite on external surfaces

	1	2	3	4	5	6	7	8	9	10
SiO_2	37.41	35.75	37.25	35.76	36.54	36.27	36.1	35.9	37.1	35.85
TiO_2	2.36	2.57	2.71	2.47	2.54	2.09	2.65	1.47	1.83	1.48
Al_2O_3	16.97	16.49	15.90	17.01	16.98	16.00	16.52	16.2	16.52	17.17
FeO	32.61	32.32	32.89	34.26	32.08	31.5	32.94	30.4	31.54	31.54
MnO	0.80	0.70	0.69	0.73	0.77	0.92	0.80	0.00	0.00	0.50
MgO	2.45	3.05	2.87	2.90	2.80	3.0	2.60	3.57	3.05	2.80
K_2O	8.81	9.00	8.81	7.78	8.94	9.10	8.93	10.2	9.16	10.2
Si	5.65	5.52	5.66	5.46	5.57	5.61	5.54	5.69	5.83	5.70
Al^{IV}	2.34	2.47	2.33	2.53	2.42	2.38	2.45	2.30	2.16	2.29
Al^{VI}	0.67	0.52	0.51	0.53	0.62	0.53	0.53	0.72	0.80	0.93
Ti	0.26	0.29	0.31	0.28	0.29	0.24	0.30	0.17	0.18	0.17
Fe	4.12	4.17	4.18	4.38	4.09	4.07	4.23	4.03	4.10	4.10
Mn	0.10	0.09	0.08	0.09	0.10	0.12	0.10	0.00	0.00	0.06
Mg	0.55	0.70	0.65	0.66	0.63	0.80	0.59	0.84	0.71	0.66
K	1.69	1.77	1.71	1.51	1.74	1.79	1.75	1.65	1.83	1.62

	11	12	13	14	15
SiO_2	36.24	36	35.4	36.5	37
TiO_2	1.29	1.57	0.74	0.74	0.74
Al_2O_3	16.5	16.44	17.08	16.5	15.08
FeO	32.15	31.26	30.42	29.3	30.09
MnO	0.42	0.00	0.00	0.00	0.00
MgO	3.00	2.80	2.65	2.50	3.50
K_2O	9.09	9.24	10.01	10.02	10.36
Si	5.65	5.67	5.67	5.82	5.90
Al^{IV}	2.35	2.32	2.32	2.17	2.10
Al^{VI}	0.68	0.72	0.89	0.92	0.73
Ti	0.15	0.18	0.08	0.08	0.08
Fe	4.19	4.11	4.07	3.91	4.01
Mn	0.05	0.00	0.00	0.00	0.00
Mg	0.69	0.65	0.63	0.59	0.83
K	1.80	1.85	2.00	2.02	2.03

two portions of fracture surfaces taken from the tested specimens are shown. For the EDS analyses, several phengite and biotite sites were localised on the surface of the polished thin sections and on the fracture surfaces. Sixty measurements of phengite crystalline phase and thirty of biotite were selected and analysed. In Figure 3A,B, two electron microscope images of phengite and biotite sites, the first in the external sample (polished thin section 1) and the second on the fracture surface (fracture surface 2), are shown.

In Tables 1 and 2, the analyses of chemical composition and atomic proportions of phengite, 30 for external surfaces (Table 1) and 30 for fracture surfaces (Table 2), are shown. In Tables 3 and 4, the analyses of biotite, 15 for external surfaces (Table 3) and 15 for fracture surfaces (Table 4), are also reported. As it is common in the analysis of phengite and biotite, the atomic proportions were computed based on 22 oxygens [11]. These atomic proportions are the most proper indicator to verify the quality of the EDS results. Based on chemical formulas of each crystalline phase, 22 oxygen atoms (44 valences) have to be counterbalanced by 44 valences of the other atoms in accordance with the overall charge neutrality of the minerals.

EDS Results for Phengite

In Figure 4A,B, the results for the Fe concentrations obtained from the measurements on phengite crystalline phase are shown. As reported in Tables 1 and 2, thirty of these measurements were carried out on the polished thin sections as representatives of the external surface samples, whereas the other thirty measurements were carried out on fracture surfaces. It can be observed that the distribution of Fe concentrations for the external surfaces, represented in the graph by squares, shows an average value of the distribution (calculated as the arithmetic mean value)

doi: 10.1111/j.1475-1305.2010.00767.x

equal to 6.20%. In the same graph, the distribution of Fe concentrations on the fracture samples (indicated by triangles) shows significant variations. It can be seen that the mean value of the distribution of measurements performed on fracture surfaces is equal to 4.0%, and it is considerably lower than the mean value of external surface measurements (6.20%). It is also interesting to note that the two Fe value distributions are separated by at least two standard deviations ($\sigma = 0.37$ in the case of external surfaces and $\sigma = 0.52$ in the case of fracture surfaces). The iron decrease, considering the mean values of the distributions of phengite composition, is about 2.20%. This iron content reduction corresponds to an absolute decrease of 35% with respect to the previous Fe content (6.20% in phengite) (see also Table 5). Similarly to Figure 4A, in Figure 4B, the Al mass percentage concentrations are considered in both the cases of external and fracture surfaces. For Al contents, the observed variations show a mass percentage increase approximately equal to that of Fe (compare Figure 4A,B). The average increase in the distribution, corresponding to the fracture surfaces (indicated by triangles), is about 2.00% of the phengite composition. The average value of Al concentrations changes from 12.50% on the external surface to 14.50% on the fracture surface. The absolute increase in Al content is equal to 16%.

The evidence emerging from the EDS analyses, that the two values for the iron decrease (–2.20%) and for the Al increase (+2.0%) are approximately equal, is really impressive. This fact is even more evident considering the trends of the other chemical elements constituting the mineral chemistry (excluding H and O) in phengite. In Figure 5A–C, the Si, Mg and K concentration distributions are reported for external and fracture surfaces. In this case, no appreciable variations can be recognised between the average values.

The evidence of Fe and Al variations in fracture samples, coming from the same specimens used for

Table 4: Chemical analyses (wt. %) and atomic proportions (basis 22 oxygens) for biotite on fracture surfaces

	1	2	3	4	5	6	7	8	9	10
SiO_2	38.84	40.65	39.28	38.5	38.50	39.50	40.01	38.60	39.71	39.21
TiO_2	2.22	2.07	2.01	2.37	2.50	2.02	2.65	1.51	1.93	1.00
Al_2O_3	18.08	19.15	19.00	19.30	18.08	19.15	18.59	19.30	18.08	19.15
FeO	25.43	25.13	25.6	26.72	26.45	27.10	28.50	28.50	26.50	22.09
MnO	0.00	0.10	0.60	0.03	0.70	0.22	0.01	0.40	0.00	0.00
MgO	4.57	4.08	4.09	4.90	4.30	4.41	4.50	4.97	3.95	4.50
K_2O	9.82	7.74	8.90	8.83	8.45	7.90	9.80	9.70	9.48	9.49
Si	5.80	5.94	5.80	5.64	5.75	5.77	5.72	5.61	5.88	5.94
Al^{IV}	2.20	2.05	2.19	2.35	2.24	2.22	2.27	2.39	2.11	2.05
Al^{VI}	0.98	1.24	1.11	0.98	0.93	1.08	0.86	0.91	1.04	1.37
Ti	0.25	0.22	0.22	0.26	0.28	0.22	0.28	0.16	0.21	0.11
Fe	3.17	3.07	3.16	3.27	3.30	3.31	3.41	3.46	3.28	2.80
Mn	0.00	0.01	0.07	0.00	0.08	0.02	0.00	0.05	0.00	0.00
Mg	1.01	0.89	0.9	1.07	0.95	0.96	0.90	1.07	0.87	1.01
K	1.87	1.44	1.67	1.65	1.61	1.47	1.79	1.79	1.79	1.83

	11	12	13	14	15
SiO_2	38.40	39.10	38.05	38.40	39.00
TiO_2	2.20	1.58	0.79	2.04	1.75
Al_2O_3	18.59	22.09	19.08	21.50	19.08
FeO	23.64	25.55	25.24	26.20	27.43
MnO	0.00	0.00	0.51	0.00	0.00
MgO	5.00	4.00	4.65	4.80	4.29
K_2O	10.69	9.11	9.20	9.20	8.20
Si	5.74	5.63	5.75	5.62	5.76
Al^{IV}	2.25	2.36	2.24	2.37	2.23
Al^{VI}	1.02	1.30	1.16	1.13	1.08
Ti	0.24	0.17	0.0	0.21	0.19
Fe	2.95	3.07	3.19	3.2	3.38
Mn	0.00	0.00	0.06	0.00	0.00
Mg	1.11	0.85	1.04	0.99	0.90
K	2.04	1.67	1.77	1.62	1.54

doi: 10.1111/j.1475-1305.2010.00767.x

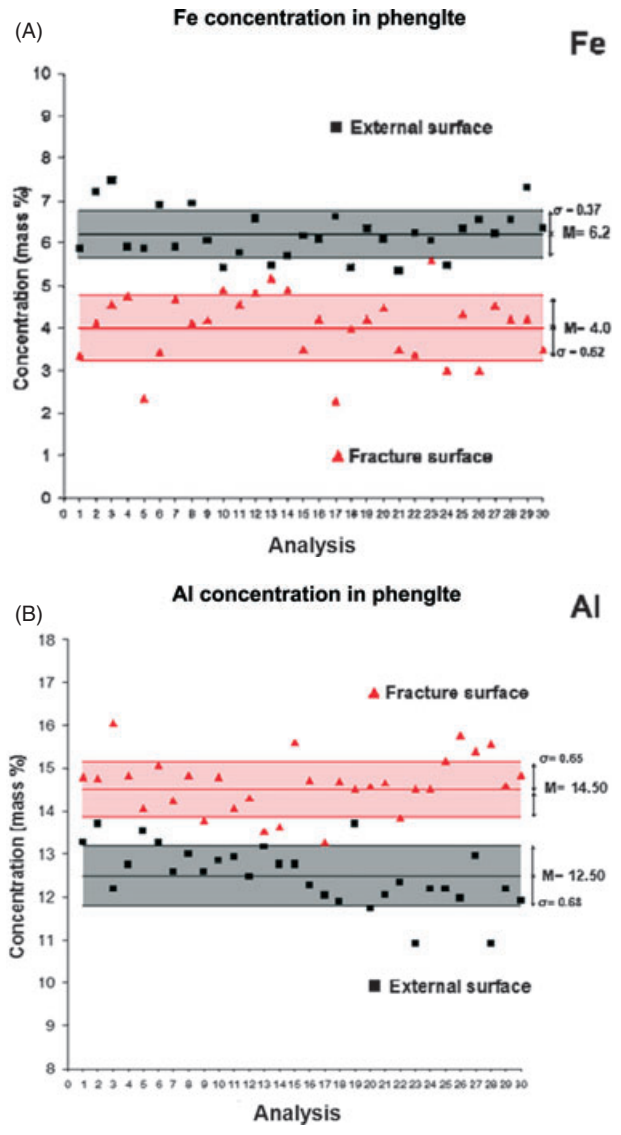

Figure 4: Fe and Al concentrations in phengite: (A) Fe concentrations for external surfaces (squares) and for fracture surfaces (triangles). The Fe decrease considering the two mean values of the distributions is equal to 2.20%. (B) Al concentrations for external surfaces (squares) and for fracture surfaces (triangles). The Al increase, considering the two mean values of the distributions, is equal to 2.00%

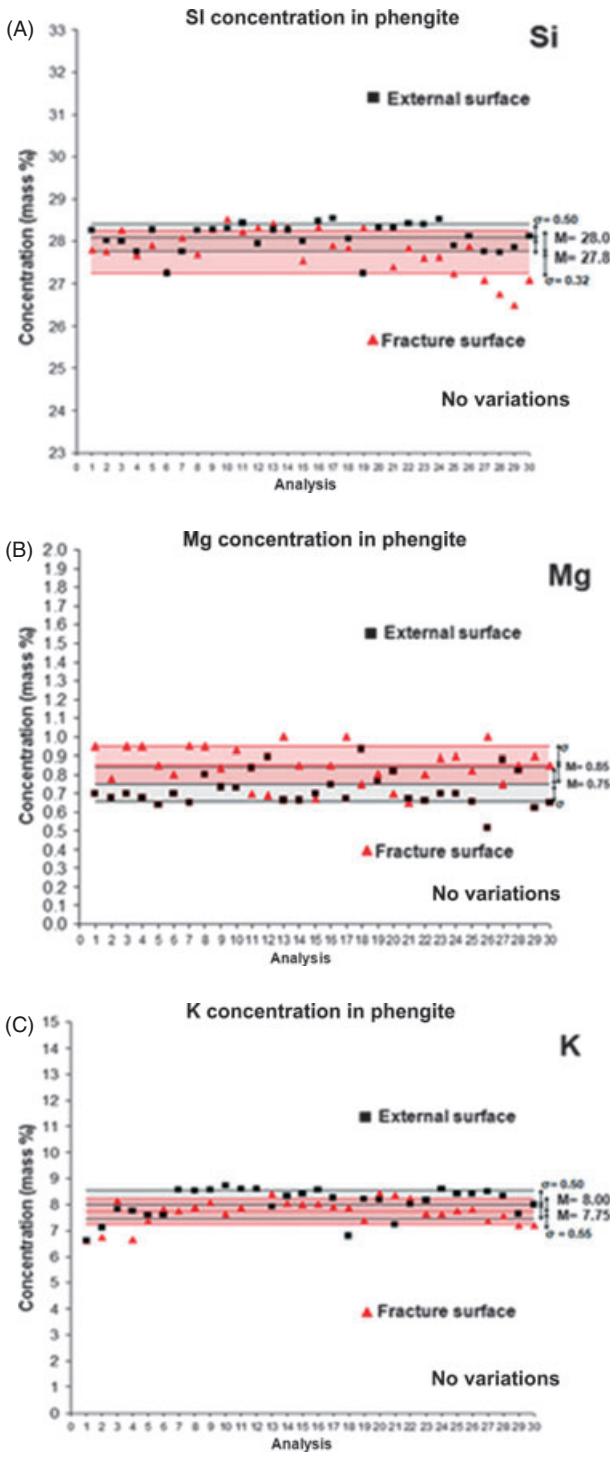

Figure 5: Si (A), Mg (B) and K (C) concentration distributions in phengite are reported for external and fracture surfaces. In this case, no appreciable variations can be recognised in fracture surfaces

Table 5: Phengite: Fe, Al, Si, Mg, and K weight percentage mean values on external and fracture surfaces. Variations with respect to the mineral (phengite) and to the same element

	External surface mean value (wt. %)	Fracture surface mean value (wt. %)	Increase/ decrease with respect to phengite	Increase/ decrease with respect to the same element
Fe	6.20	4.00	−2.20%	−35%
Al	12.50	14.50	+2.00%	+16%
Si	28.00	27.80	No variations	No variations
Mg	0.75	0.85	No variations	No variations
K	8.00	7.75	No variations	No variations

piezonuclear tests [4, 5], together with the neutron emission measurements reported by Carpinteri *et al.* [4] and by Cardone *et al.* [5], leads to the conclusion that the piezonuclear reaction:

$$\mathrm{Fe}_{26}^{56} \rightarrow 2\,\mathrm{Al}_{13}^{27} + 2 \text{ neutrons} \qquad (1)$$

should have occurred [4, 5, 8].

doi: 10.1111/j.1475-1305.2010.00767.x

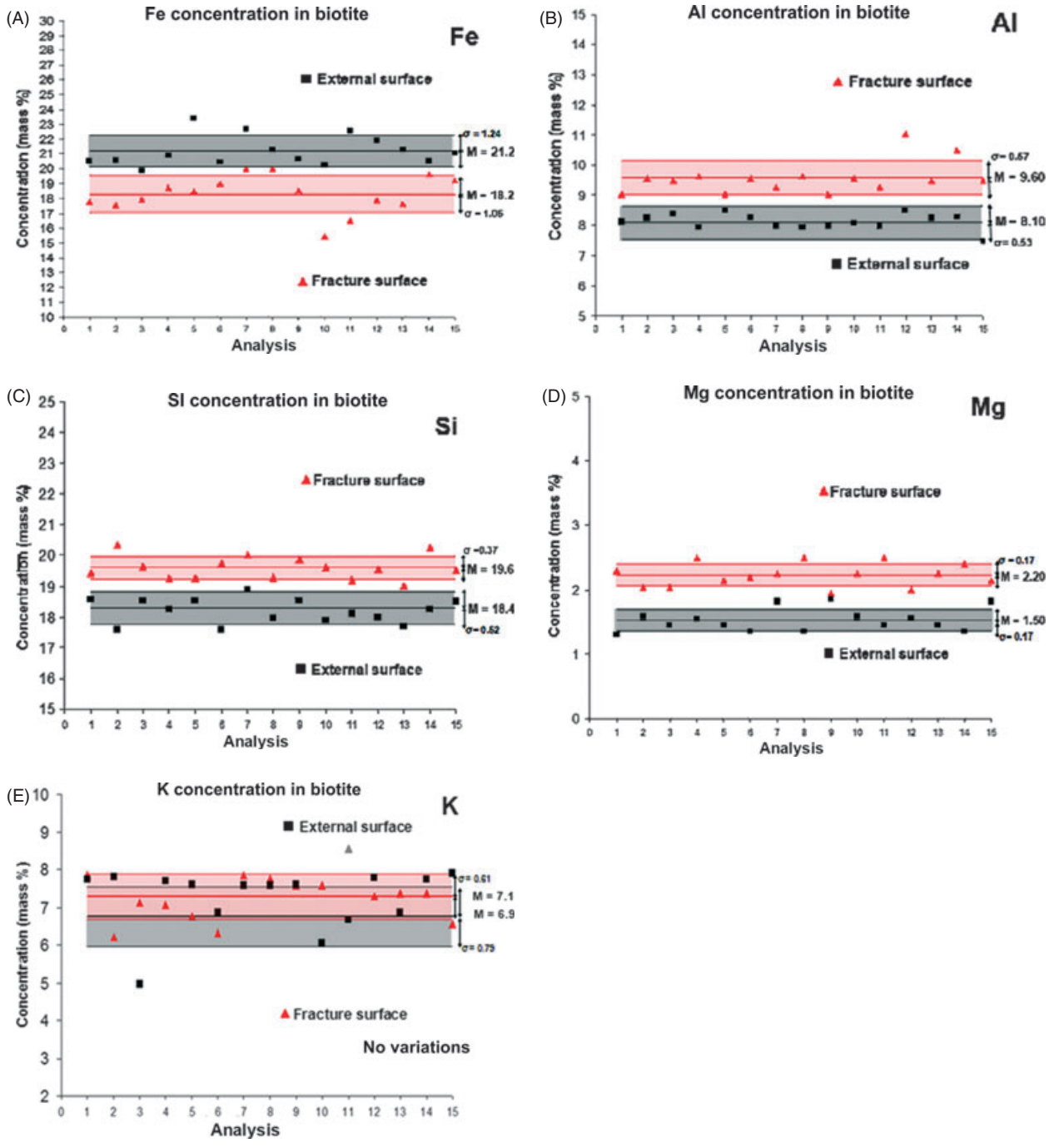

Figure 6: Fe (A), Al (B), Si (C), Mg (D) and K (E) concentrations in biotite are reported for external and fracture surfaces. The iron decrease (−3.00%) in biotite is counterbalanced by an increase in aluminium (+1.50%), silicon (+1.20%) and magnesium (+0.70%). In the case of K, no appreciable variations can be recognised between the external and the fracture samples (see also Table 6)

EDS Results for Biotite

In the Figure 6A–E, the results for Fe, Al, Si, Mg and K concentrations measured on 30 acquisition points of biotite crystalline phase are shown (see also Tables 3 and 4). These measurements were selected on the polished thin sections as representatives of the uncracked material samples (15 measurements) and of fracture surfaces (15 measurements). It can be observed that the distribution of Fe concentrations for the external surfaces, represented in Figure 5A by squares, shows an average value of the distribution (calculated as the arithmetic mean value) equal to 21.20%. On the other hand, considering in the same graph the distribution of Fe concentrations on fracture samples (indicated by triangles), it can be seen that the mean value drops to 18.20%. In this case, the iron decrease, considering the mean values of the distributions of biotite composition, is about 3.00%. This iron content reduction (−3.00%) corresponds to an absolute decrease of 14% with respect to the previous Fe

doi: 10.1111/j.1475-1305.2010.00767.x

Table 6: Biotite: Fe, Al, Si, Mg, and K weight percentage mean values on external and fracture surfaces. Variations with respect to the mineral (biotite) and to the same element

	External surface mean value (wt. %)	Fracture surface mean value (wt. %)	Increase/ decrease with respect to biotite	Increase/ decrease with respect to the same element
Fe	21.20	18.20	−3.00%	−14%
Al	8.10	9.60	+1.50%	+18%
Si	18.40	19.60	+1.20%	+6%
Mg	1.50	2.20	+0.70%	+46%
K	6.90	7.10	No variations	No variations

content (21.20% in biotite) (see Table 6). Similarly to Figure 6A, in Figure 6B the Al mass percentage concentrations are considered in both cases of external and fracture samples. For Al contents, the observed variations show an average increase of about 1.50% in the biotite composition. The average value of Al concentrations changes from 8.10% on the external surface to 9.60% on the fracture surface, with an absolute increase in Al content equal to 18%. In Figure 6C,D, it is shown that, in the case of biotite, also Si and Mg contents present considerable variations, whereas only K does not show appreciable variations (Figure 6E). Figure 6C shows that the mass percentage concentration of Si changes from a mean value of 18.4% (external surface) to a mean value of 19.60% (fracture surface) with an increase of 1.20%. Similarly, in Figure 6D, the Mg concentration distributions show that the mean value of Mg content changes from 1.50% (external surface) to 2.20% (fracture surface). Therefore, the iron decrease (−3.00%) in biotite is counterbalanced by an increase in aluminium (+1.50%), silicon (+1.20%) and magnesium (+0.70%). Considering these evidences for the biotite content variations in Fe, Al, Si and Mg, in analogy to the results of EDS analyses discussed in the previous section, it is possible to conjecture that another piezonuclear reaction, in addition to (1), should have occurred in biotite crystalline phase during the piezonuclear tests [4, 5, 8]:

$$\mathrm{Fe}_{26}^{56} \rightarrow \mathrm{Mg}_{12}^{24} + \mathrm{Si}_{14}^{28} + 4 \text{ neutrons} \qquad (2)$$

Conclusions

Energy-dispersive X-ray spectroscopy was performed on different samples of external and fracture surfaces belonging to specimens used in the piezonuclear tests recently reported in Carpinteri *et al.* [4] and Cardone *et al.* [5]. For each sample, different measurements of the same crystalline phases (phengite or biotite) were performed to obtain averaged information of their chemical composition and to detect possible piezonuclear transmutations from iron to lighter elements. Considering the results for phengite and biotite, and also their abundances in the Luserna stone composition, a considerable reduction in the iron content (∼25%) is observed. This iron decrease is counterbalanced by an increase in aluminium, silicon and magnesium. In particular, the increase in aluminium content corresponds to the 85 per cent of the iron decrease. Therefore, the author's opinion is that piezonuclear fission reactions (1) and (2) should have occurred in granitic gneiss during the piezonuclear tests [4, 5]. Finally, considering that granite is characterised by an extensive concentration in the rocks that make up the Earth's continental crust (∼60% of the Earth's continental crust), the piezonuclear fission reactions considered above can be generalised from the laboratory to the Earth's crust scale, where mechanical phenomena of brittle fracture, because of tectonic activity, take place continuously in most seismic areas [17].

ACKNOWLEDGEMENTS

The financial support provided by Regione Piemonte (RE-FRESCOS project) is gratefully acknowledged. The authors would like to thank Prof. F. Pirri and Dr S. Guastella of the Department of Materials Science and Chemical Engineering (Politecnico di Torino) for their kind collaboration in the EDS analysis. Special thanks are also due to Prof. Alessandro Borghi of the Department of Mineralogical and Petrological Sciences (Università di Torino) for his helpful discussions and suggestions on chemical and atomic proportion analyses.

REFERENCES

1. Arata, Y. and Zhang, Y. (1995) Achievement of solid-state plasma fusion ('cold-fusion'). *Proc. Jpn. Acad. Ser. B*, **71**, 304–309.
2. Arata, Y., Fujita, H. and Zhang, Y.-C. (2002) Intense deuterium nuclear fusion of pycnodeuterium-lumps coagulated locally within highly deuterated atom clusters. *Proc. Jpn. Acad. Ser. B*, **78**, 201–204.
3. Taleyarkhan, R. P., West, C. D., Cho, J. S., Lahey, R. T., Jr, Nigmatulin, R. I. and Block, R. C. (2002) Evidence for nuclear emissions during acoustic cavitation. *Science* **295**, 1868–1873.
4. Carpinteri, A., Cardone, F. and Lacidogna, G. (2009) Piezonuclear neutrons from brittle fracture: early results of mechanical compression tests. *Strain* **45**, 332–339, Presented also at the Turin Academy of Sciences on December 10, 2008, Proc. of the Turin Academy of Sciences, Ser. V, (2010) 33: 27–42.

doi: 10.1111/j.1475-1305.2010.00767.x

5. Cardone, F., Carpinteri, A. and Lacidogna, G. (2009) Piezonuclear neutrons from fracturing of inert solids. *Phys. Lett. A.* **373**, 4158–4163.
6. Cardone, F., Cherubini, G. and Petrucci, A. (2009) Piezonuclear neutrons. *Phys. Lett. A.* **373**, 862–866, See also: F. Cardone *et al*. http://www.arxiv.org/abs/0710.5115.
7. Cardone, F. and Mignani, R. (2007) *Deformed Spacetime*. Springer, Dordrecht, Chapters 16–17.
8. Carpinteri, A., Lacidogna, G., Manuello, A. and Borla, O. (in press) Neutron emissions in rock specimens under monotonic, cyclic, and vibrational loading. *Strain*.
9. Vola, G. and Marchi, M. (2009) Mineralogical and petrographic quantitative analysis of a recycled aggregate from quarry wastes. The Luserna stone case-study. *Proc of the 12th Euroseminar on Microscopy Applied to Building Materials*, 15–19 September 2009, Dortmund, Germany.
10. Sandrone, R., Cadoppi, P., Sacchi, R. and Vialon, P. (1993) The Dora-Maira Massif. In: *Pre-Mesozoic geology in the Alps*. (J. F. Von Raumer and F. Neubauer, Eds). Springer, Berlin: 317–325.
11. Sandrone, R. and Borghi, A. (1992) Zoned garnets in the northern Dora-Maria Massif and their contribution to a reconstruction of the regional metamorphic evolution. *Eur. J. Minerals* **4**, 465–474.
12. Compagnoni, R., Crisci, G. M. and Sandrone, R. (1982–1983) Caratterizzazione chimica e petrografica degli ''gneiss di Luserna'' (Massiccio cristallino Dora-Maira, Alpi Occidentali). *Rend. Soc. It. Min. Petr.* **38**, 498.
13. Sandrone, R. (2001) La Pietra di Luserna nella letteratura tecnico-scientifica. Sem. Int. Le Pietre Ornamentali della Montagna Europea, Luserna San Giovanni-Torre Pellice (TO), 10–12 giugno 2001, 333–339.
14. Carpinteri, A. (1989) Cusp catastrophe interpretation of fracture instability. *J. Mech. Phys. Solids* **37**, 567–582.
15. Carpinteri, A. (1990) A catastrophe theory approach to fracture mechanics. *Int. J. Fract.* **44**, 57–69.
16. Carpinteri, A. and Corrado, M. (2009) An extended (fractal) overlapping crack model to describe crushing size-scale effects in compression. *Eng. Fail. Anal.* **16**, 2530–2540.
17. Carpinteri, A. and Manuello, A. Geomechanical and geochemical evidence of piezonuclear fission reactions in the Earth's crust. *Strain*. doi: 10.1111/j.1475-1305.2010.00766.x